Lab on a Chip

PAPER

View Article Online
View Journal | View Issue

Cite this: *Lab Chip*, 2014, **14**, 2480

A high-efficiency microfluidic device for size-selective trapping and sorting†

Jinho Kim,*[a] Jessey Erath,[b] Ana Rodriguez[b] and Changhuei Yang[ac]

Received 20th February 2014,
Accepted 7th May 2014

DOI: 10.1039/c4lc00219a

www.rsc.org/loc

We report the development of a simple poly(dimethylsiloxane) microfluidic device for high-efficiency trapping and sorting of micron-size particles. In this device, hydrodynamic fluid flow through the sieve-like microfluidic channel sequentially fills the trap positions with particles of the trap size, and particles smaller than the trap size pass through the sieve and are trapped by smaller traps downstream. By incorporating side channels alongside the main channel, we were able to decouple the fluidic flow in one stage from the flows in the other stages. This decoupling allows us to modularize each stage of the device regardless of the size of the entire device. In our demonstration experiment with the prototype, we showed that more than 85% of the polystyrene microspheres (of sizes 15 μm, 6 μm and 4 μm) were sorted in the correct segment of the device that targets their respective sizes. Moreover, this high-efficiency device was able to trap all microspheres which were introduced into the device. Finally, we tested the device's ability to trap and sort three different species of waterborne parasites (*Entamoeba*, *Giardia*, and *Cryptosporidium*) and obtained excellent sorting performance.

Introduction

Microenvironments built in microfluidic systems provide excellent conditions for single-cell experiments due to the controllability of various culturing factors inside the system.[1] For such microenvironments to be useful in biological and chemical experiments, samples should be efficiently and accurately located at the designated positions. Many types of single-cell trapping methods have been developed to address this issue.[2,3] These methods can be classified fundamentally into five categories: chemical, hydrodynamic, optical, acoustic, and magnetic trapping. Among them, hydrodynamic trapping is the most common and simplest way to realize cell or particle trapping in the microfluidic system.[3] Di Carlo *et al.* built barriers against the fluid flow and used the stagnation points made by these barriers as a "shielded" trap region.[4] Once the cells were trapped successfully at the barriers, this shielded region constrained the cells in an isolated experimental environment. However, the trapping efficiency of this barrier method is usually low, because this stagnancy actually discourages the cells from moving into the traps. An improvement to this barrier method was made by Wlodkowic *et al.*[5] They created small gaps in the barriers to increase flow rate into the trap region and thereby reduced the stagnancy associated with unoccupied traps. Even with this enhanced flow into the trap region, the reported trapping efficiency of the sample cells was between 10% and 20%.[5] In other words, most of the samples were still lost during the trapping procedure. Tan and Takeuchi employed a different approach to perform hydrodynamic particle trapping.[6,7] They used fluidic resistance along the different paths in the microfluidic channel to carry microbeads into the trap. They manipulated the flow into the each trap position and successfully carried all of their test sample beads sequentially into the traps. However, their device was designed to trap particles of a specific size, and the particle trapping characteristics could change significantly when a mixture of beads that exhibits a wide size variation was used in the same device.[6] Unsurprisingly, microfluidic trapping and particle size sorting[8–10] are generally implemented as separate systems.

This paper reports our recent work on the design and implementation of a high efficiency, trapping-and-sorting microfluidic device. Such a device is highly desired for working with a range of biological field samples. One such application is the harvesting and identification of waterborne protozoan parasites from suspected water sources. In such applications, the concentration of the suspected targets can be extremely low without any treatment. For example, the concentration of *Giardia* cysts, a type of waterborne

[a] *Department of Electrical Engineering, California Institute of Technology, 1200 E. California Blvd., Pasadena, CA, 91125, USA. E-mail: jkkim@caltech.edu; Fax: +1(626) 3958475; Tel: +1(626) 3952258*
[b] *Department of Microbiology, Division of Medical Parasitology, New York University School of Medicine, New York, NY, 10010, USA*
[c] *Department of Bioengineering and Medical Engineering, California Institute of Technology, 1200 E. California Blvd., Pasadena, CA, 91125, USA*
† Electronic supplementary information (ESI) available. See DOI: 10.1039/c4lc00219a

protozoan parasite that causes acute diarrhea in infected people, is as low as 20 cysts per liter of raw, polluted water.[11] As a result, high trapping efficiency is required for the successful field application of the microfluidic trapping device. Another parameter that should be considered about the field sample is the impurity of the sample. Samples from the field can contain many different sizes of materials. For example, four different species of protozoan parasites (*Entamoeba*, *Giardia*, *Cryptosporidium*, and *Cyclospora*) along with other debris should be identified to determine the main source of waterborne infection. Diagnosis of these four diseases is currently performed by microscopic examination. Even though the cysts can be stained with different dyes, it is time consuming to mount and scan all the samples manually and often yields negative results due to the small number of cysts in the sample.[12] If these cysts can be located at specific locations within a device, the time of diagnosis would be reduced significantly.

In this paper, we introduce a microfluidic trapping device that can allocate particles to different trap zones by size. This device uses fluid flow rate differences through different paths made by the traps similar to those of the Tan and Takeuchi device.[6] As a result, the trapping efficiency of the device can be manipulated by controlling the channel dimensions of the device. In addition, size sorting is achieved through the gaps in the trap positions. To enable both trapping and sorting to work at the same time, additional side channels were added to isolate and decouple fluid flow between each stage in the device. A detailed explanation about the configuration and working principles of the microfluidic trapping device is found in the Results and discussion section, followed by a computational fluid dynamics simulation analysis for the understanding of the fluid flow patterns inside the device and the optimal design parameter selection of the device. Experimental results using polystyrene beads and waterborne parasites demonstrate the working mechanism of the fabricated device. The device fabrication and parasites preparation methods are summarized in the Methods section and Conclusions are found at the end of the paper.

Results and discussion

Device configuration

Our microfluidic device is shown in Fig. 1(a). The microfluidic trapping prototype is composed of three different sized trap zones connected sequentially from the inlet. Zone A is designed for large particle trapping (target particle diameter: 15 μm), zone B is for medium-sized particle trapping (target particle diameter: 6 μm), and zone C is for small particle trapping (target particle diameter: 3 μm). Each zone

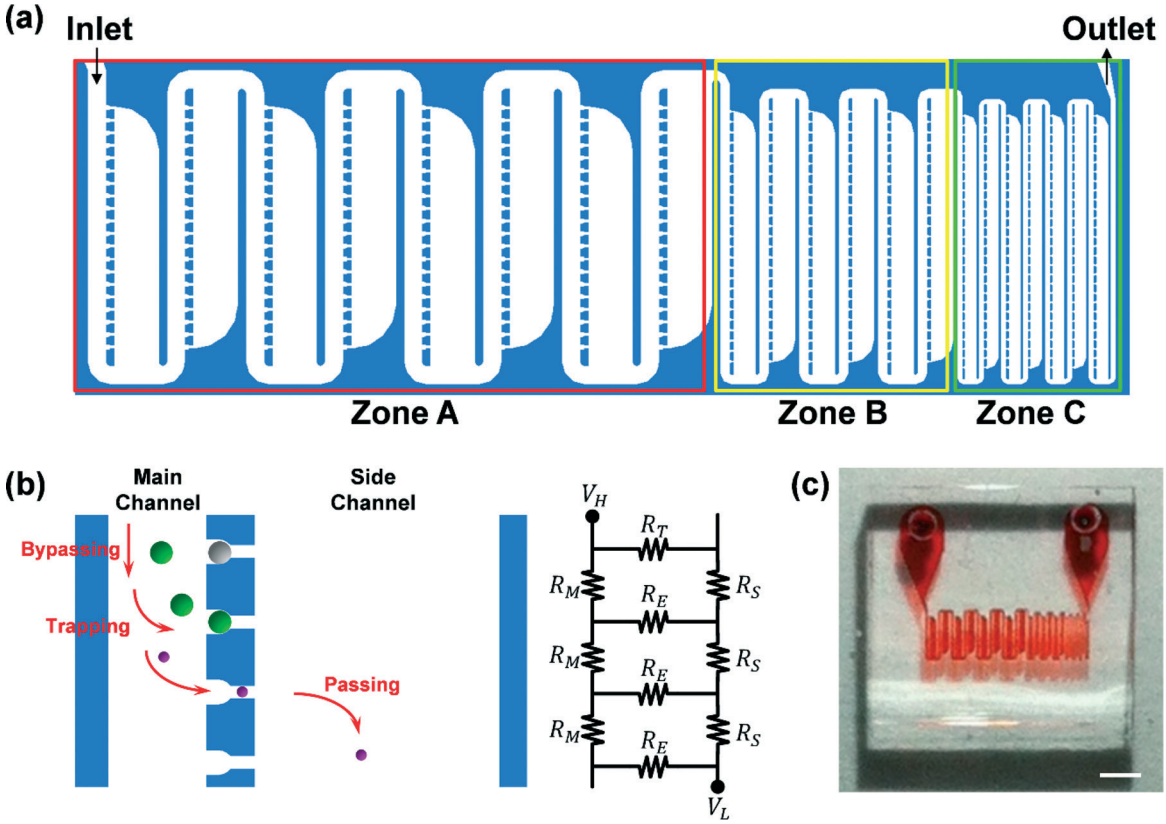

Fig. 1 Microfluidic trapping device for three different sizes of particles. (a) Trap positions for large (zone A), medium (zone B), and small (zone C) particles. (b) Schematic diagram for the trapping and passing mechanisms (left) and circuit representation of particle flow (right). R_M: fluidic resistance of the main channel, R_S: fluidic resistance of the side channel, R_T, R_E: fluidic resistance of the trap that is filled or empty, respectively, V_H, V_L: highest and lowest potential nodes, respectively. (c) Photograph of the device. Scale bar: 1 mm.

consists of the main channel, traps, and side channels as shown in Fig. 1(b). The basic mechanism of particle trapping and size sorting is similar to that of the sieve. Particles smaller than the trap gap size pass through the trap, whereas particles larger than the gap size are trapped geometrically. Here, we use the fluidic pressure difference as the main force for inducing particles into the trap. The side channels in our device play critical roles in the multiple-trap configuration in a fluidic stage and the size sorting of particles through different stages. Without the side channels, leakage from occupied traps would directly enter the main channel of the next stage and make the analysis of the fluidic flow pattern in the partially occupied device significantly more difficult. To suppress these fluidic flow coupling effects, Tan and Takeuchi constructed detours of the main channel;[7] however, such a method merely reduces the coupling of fluidic flow between stages and does not remove it. Furthermore, the size of the detour is too large for the working area of the device (a 1.8 to 3.6 mm length detour for 100 μm microsphere samples).[7] In our device, the side channels effectively isolate the leakage flow from the main channel of the next stage, and no such detours are needed. Furthermore, particles of varied sizes flow in a regular and controllable pattern without counterflow with the help of the decoupling of fluidic flow by the side channels. This process enables small particles to be under constant fluidic flow conditions regardless of the positions of the stages. The trapping principle of our microfluidic device can be easily understood using the circuit representation of fluid flow inside the device [Fig. 1(b)]. If we assume that the particles inside the fluid follow the fluid flow direction inside the microfluidic channel, particle trapping efficiency will be proportional to the flow rate into the side channel. Fluid pressure differences between the channels is determined by the input/output conditions and the fluidic resistance of the channel; the fluidic resistance of the empty trap (R_E) is fixed by the dimension of the target particles. As a result, the remaining design parameters that can be controlled for maximum flow rate into the side channels are the fluidic resistance of the side channels (R_S) and main channels (R_M). Fluidic resistance through a rectangular channel is represented by its channel dimension as:[6]

$$R = \frac{C(\alpha)}{32} \cdot \frac{\mu L P^2}{A^3} \quad (1)$$

where $C(\alpha)$ is a constant that is a function of channel aspect ratio (α), μ is the fluid velocity, L is the length of the channel, P is the perimeter of the channel, and A is the cross-sectional area of the channel. From eqn (1), the simplest way to reduce fluidic resistance of a fixed-height channel is to increase the width of the channel. As a result, we can increase the particle trapping efficiency of the device by manipulating each channel width accordingly. Furthermore, this fluidic resistance at the trap works as a variable resistance for the bypassing function from the already occupied trap. Once a trap is occupied by a correctly sized particle, the path through the trap is blocked, and the cross-sectional area of the trap is significantly reduced. This increases fluidic resistance of the trap from a low value (R_E) to a high value (R_T). As a result, flow into the occupied trap is reduced and the next particle bypasses the occupied trap and flows into the next empty trap automatically. The actual dimensions of the microfluidic device are listed in Table 1 (W_T: trap size, W_G: passing gap size, W_{ch}: main channel width, W_{side}: side channel width, H: channel height). The criteria for deciding specific channel dimensions will be discussed in the Simulation results section. A photograph of the fabricated microfluidic channel filled with red ink is shown in Fig. 1(c). The size of the entire trap region is about 4 mm × 1 mm, and 160, 150, and 196 traps exist in zones A, B, and C, respectively.

Simulation results

To better understand the flow characteristics around the microfluidic traps and to determine the optimal parameters for microfluidic channel design, a computational fluid dynamics (CFD) analysis was carried out using COMSOL 4.3 (COMSOL Multiphysics). We used the dimensions of Zone A in Table 1 for the design of the simulation, and a 3D laminar flow CFD model was used for the calculation. The fluid material inside the channel was water, and we applied an incompressible flow model to the fluid. No slip conditions were imposed on the channel walls, and the input/output boundary condition was set by the fluid velocity (V_{in} = 10 mm s^{-1}) and pressure (P_{out} = 0), respectively. The environmental temperature was T = 293.15 K. Cross-sectional profiles at the center plane of the microfluidic device are shown in Fig. 2. From the velocity profile in Fig. 2(a), it is clear that flow patterns are periodically repeated for each new stage in the traps. It is easily understandable, considering the configuration of the channel. The microfluidic channel is basically one long serial path that periodically separates and recombines as the flow passes through the traps. Because the width of the main channel is fixed throughout the channel and flow is incompressible, the fluid velocity before channel separation should be the same as the velocity after channel reunion. As a result, the fluid is subjected to exactly the same conditions when each new stage of the channel begin (if we can ignore the loss from the wall). This means that we do not need to consider the entire system's flow characteristics but only one stage of the channel when we enlarge the system. Once the flow patterns of one zone are specified from the simulation, those of the other zones can be estimated using Reynolds number.[13] The Reynolds number of the flow inside rectangular channel is defined as:

Table 1 Geometric dimensions of microfluidic traps (unit: μm)

	W_T	W_G	W_{ch}	W_{side}	H
Zone A	16	8	64	160	22
Zone B	8	4	32	80	22
Zone C	4	2	16	40	22

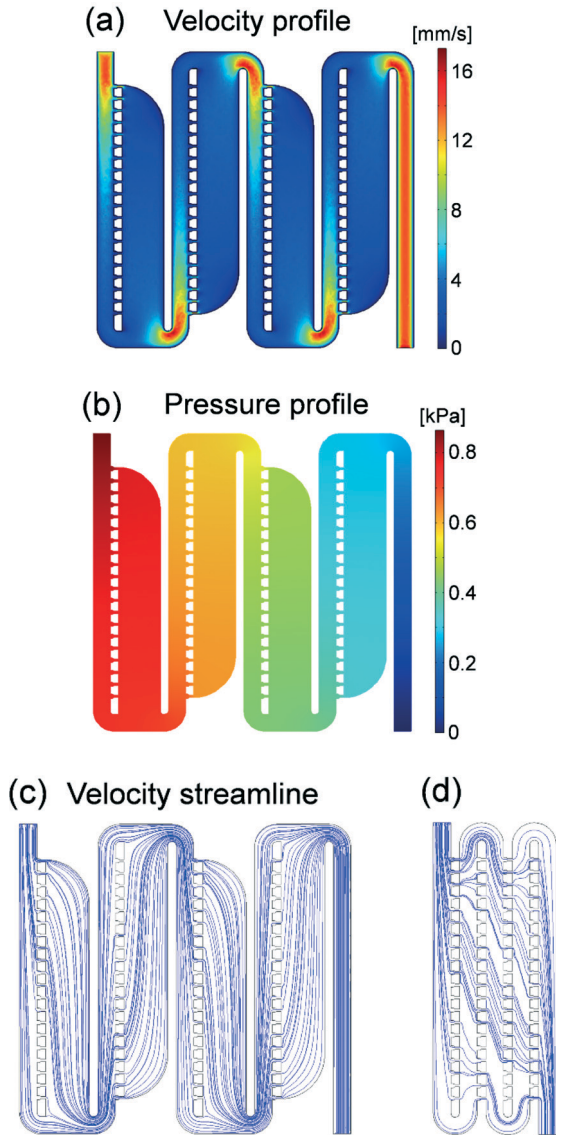

Fig. 2 Computational fluid dynamic simulation. (a) Velocity profile. (b) Pressure profile. (c and d) Velocity streamline through the microfluidic traps with and without side channels.

$$\mathrm{Re} = \frac{\rho V D_{\mathrm{H}}}{\mu} = \frac{\rho V}{\mu}\frac{2WH}{W+H} \tag{2}$$

where ρ is the density of the fluid, V is the mean velocity of the fluid, and D_{H} is the hydraulic diameter that is determined by the shape of the channel. In our device, we reduced the width (W) of the channel in zone B to one-half of the width of the channel in zone A while fixing the height (H) of the channels. As a result, fluid velocity (V) increased by twice in zone B while the hydraulic diameter was unable to be reduced by one-half, resulting in an increase of the Reynolds number. If the dimensions in Table 1 are used to calculate the Reynolds number, the Reynolds numbers in zones B and C are 1.5 and 2.1 times larger than that in zone A, respectively. However, the maximum Reynolds number calculated for zone A was 0.0623, which is much smaller than 2000, even allowing for an increase in the Reynolds number in zone C. Therefore, we assume that fluid flow inside the whole device is highly laminar and ignore irregularities from the turbulence inside the channel. The pressure profile at the center plane of the microfluidic channel is shown in Fig. 2(b). The pressure decreases along the main channel of the device, and the pressure at the main channel is always higher than the pressure at the side channel of the same position. These two results mean that there is no counter-flow inside the channel and fluids from the main channel flow into the side channel all the way. Fluid flow inside the microfluidic channel is more evident from the velocity streamline as shown in Fig. 2(c). For comparison, the velocity streamline of same-sized channel that doesn't have side channels is shown in Fig. 2(d). Without side channels, fluid flows in the each stage are coupled together and the flow pattern is different in every stage. Furthermore, there are counter-flows in the second and fourth stages from the inlet, meaning that particles from the inlet cannot flow into next stage across the counter-flows, resulting in the channel clogging in these counter-flow stages. Chung *et al.* made a microfluidic trap design similar to that shown in Fig. 2(d).[14] However, their design was mainly for the orientation of elliptically shaped samples not for size sorting. For that purpose, they utilized a narrow gap width to increase the fluidic resistance of the empty trap region. However, for size sorting, the trap gap width cannot be that narrow for small particles to pass through. In our design, we were able to isolate and decouple fluid flow in each stage with the help of side channels, and highly regular fluid flow patterns were made in every stage, allowing fluid to actually flow into the side channels from the main channel, as can be seen in Fig. 2(c).

Until now, we only simulated the fluid flow pattern inside the microfluidic channel; however, the actual trapping is made by the flow of the particles inside the fluid. The tendency for particle tracing on the fluid flow is represented by the Stokes number. The Stokes number is defined as the ratio of the particle response time and fluid flow characteristic time.[15] If the Stokes number is much smaller than 1, the particle responses are much faster than the change in fluid flow. As a result, the particles inside the fluid will have a nearly equal velocity profile to the fluid in the channel. In a low Reynolds number regime, the Stokes number can be represented as:[16]

$$\mathrm{Stk} = \frac{\rho_{\mathrm{p}} d_{\mathrm{p}}^{2} V}{18\mu d_{\mathrm{c}}} \tag{3}$$

where ρ_{p} is the density of the particle, d_{p} is the diameter of the particle, and d_{c} is the characteristic dimension of the obstacle. In our device, fluid flows are divided by the walls between the traps. If we use the distance between the traps (30 μm) as d_{c} for the calculation, the Stokes number in zone A is about 0.007 (in case of polystyrene, ρ_{p} = 1050 kg m^{-3}). Considering that the particle size in zone B will be smaller than one-half of the particle in zone A and the fluid velocity

in zone B is twice than the fluid velocity in zone A, we can estimate that the Stokes number in zone B will be smaller than one-half of 0.007. Furthermore, the Stokes number in zone C will be smaller than that in zone B. Because the Stokes number in our device is much smaller than 1 in all zones, the particles in our device will follow fluid flow faithfully inside the channel.

From Fig. 2(c), we can see that much of the fluid flows through the side channels; however, we need to know exactly how much of the total fluid flows through each trap to determine the trapping efficiency in each trap position. To that purpose, we defined relative flow rate by:

$$\text{Relative flow rate} = \frac{\text{Flow rate though each trap}}{\text{Total flow rate}}.$$

From this definition, we can determine how much fluid flows through a specific trap position. The relative flow rates through each trap position from the inlet are shown in Fig. 3 by several design variations. The higher the relative flow rate at a trap means the greater chance to trap particles at that position. In Fig. 3(a), relative flow rate distributions through traps in one stage of the channel are shown by different main channel widths. All other design variables except the one under consideration were fixed for this simulation. As the main channel width becomes narrower, the relative flow rate through the first trap position increases. This is because the fluidic resistance in the main channel (R_M) increases by decreases of the channel width, whereas the other fluidic resistances (R_E, R_S) remain the same. However, this flow rate trend cannot be used directly for particle trapping efficiency, because this simulation does not consider particle size in the microfluidic channel. To assess fluid flow patterns when a particle is inside the channel, fluid velocity streamlines when a target-sized particle is on the edge of a trap are shown in Fig. 3(a) (in cases where the main channel widths are 1 and 4 times the trap width). Even though the relative flow rate through the first trap position is high in the case of a narrow channel, the main flow direction of the particle is into the main channel, not into the side channel, because the particle size is too large compared with the main channel width. For a particle to receive effective drag forces into the side channel, the region where fluid flows into the side channel should be larger than the particle size. In the case of a wide channel, it is clear that fluid flows across the particle into the side channel, which directs the particle into the trap. From the experimental tests, optimal trapping results were observed in the case of main channel width 4 times the trap width. The relative flow rate slightly increases through all the traps, as side channel widths increase, as shown in Fig. 3(b). This is because the fluidic resistance of the side channels (R_S) is connected serially with the fluidic resistance of the trap (R_E), and R_E is much higher than R_S. As a result, the effect of decreasing R_S is not as distinct as that of decreasing R_M. To obtain better trapping efficiency, we chose the width of the side channels to be 2.5 times the main channel width. Using

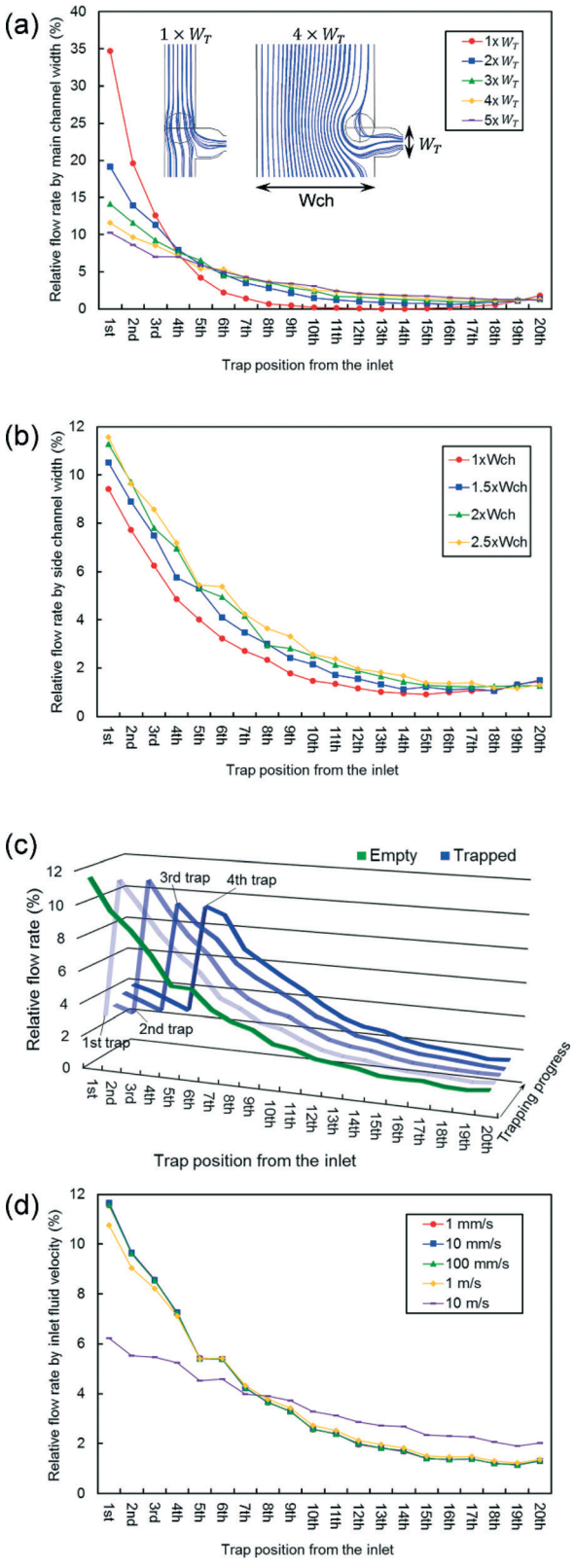

Fig. 3 Flow rate dependence on the microfluidic channel design parameters. (a) Relative flow rate through the traps by main channel width. (b) Relative flow rate through the traps by side channel width. (c) Relative flow rate change as particle trapping progresses. (d) Relative flow rate through the traps by inlet fluid velocity.

optimal design parameters determined from the simulation, progressive particle trapping effects on relative flow rates were assessed as shown in Fig. 3(c). We assumed that the particle will be directed into the trap of the highest relative flow rate at the point of trapping and inserted a spherical barrier inside the trap sequentially from the inlet for such a simulation. In the beginning, there were no particles inside the channel and the flow pattern was the same as before. When the first particle was located inside the first trap position, the relative flow rate in the first trap decreased dramatically and the second trap had the highest relative flow rate. When the second particle was positioned at the second trap, the relative flow rate in the second trap decreased and the third trap had the highest relative flow rate. These changes in flow rate continued until the last trap was filled with particles. In this way, particles inside the channel were automatically directed to and filled the empty trap.

Until now, we determined the optimal design criteria for our microfluidic device from several simulation results under fixed boundary conditions. To determine which of these conditions caused flow patterns to deviate from normal values, similar simulations were made using different inlet fluid velocities, as shown in Fig. 3(d). When the inlet fluid velocity was decreased or increased by one order of magnitude from the normal velocity (V_{in} = 10 mm s^{-1}), the difference in the fluid flow pattern was negligible. When the inlet fluid velocity was increased by two orders of magnitude, the relative flow rate was slightly reduced at the first and second trap positions, but the entire flow pattern did not change significantly. However, the relative flow rate at the first trap position was reduced by one-half, and the flow rates at the downstream positions increased when the inlet fluid velocity increased by three orders of magnitude. Under this input condition, the maximum Reynolds number was calculated to be 57.8. Based on this number, the fluid flow began to change into turbulent flow, and irregularities of this turbulent flow changed the flow pattern inside the microfluidic channel. From a practical point of view, however, it is virtually impossible to induce such a high fluid velocity inside a microfluidic channel, mainly due to wall resistance. As a result, we think that our device can operate at a wide range of input boundary conditions and is highly tolerant of fluctuations from the external environment.

Experimental results

A microfluidic trapping device was constructed using micro fabrication methods. We used poly(dimethylsiloxane) (PDMS) as the channel material and bonded the channel to the slide glass. The specific dimensions of the microfluidic channel were based on the results of the simulations. All design parameters were based on the following sequences. First, the target particle size for each zone was decided. The height of the channel was chosen to be 30% larger than the largest possible particle to avoid channel clogging. The main channel width was determined from the particle size multiplied by 4. The side channel width was determined using the main channel width multiplied by 2.5. The trap gap width of each zone was determined to be slightly larger than the size of the particle in the next zone. The dimensions calculated using these sequences are shown in Table 1. The fabricated device was connected to a syringe using Tygon tubing, and samples inside the syringe were pushed into the microfluidic channel using a syringe pump (Harvard Apparatus). Polystyrene microspheres were used for sample particles, and the infusion rate of the syringe pump was set as 1 μl min^{-1}. Fig. 4 shows an image of microsphere trapping inside the channel over time using a 4×/0.10 objective lens. The samples were made up of mixtures of 15 μm sized polystyrene microspheres (Polysciences, Inc. #18328) at 10^5 ml^{-1} concentration and 4.5 μm sized polystyrene microspheres (Polysciences, Inc. #17135) at the same concentration in a volume ratio of 3 : 1. At the first time point, three 15 μm microspheres had already occupied the traps and a new 4.5 μm microsphere passed by the filled traps and went to the next zone. At T = 1.3 s and 2.4 s, new 15 μm microspheres filled the next empty traps. At T = 7.0 s, a new 4.5 μm microsphere appeared in the channel and passed the trap and went to the next zone. We checked that these 4.5 μm microspheres were trapped in zone B of the device. Time sequence images confirmed that our device works well with regard to the bypassing, trapping, and sorting functionalities. The real-time videos showing trapping in zones A and B are available as ESI.†

Similar experiments were performed using fluorescent microspheres to assess the distribution of the trapped microspheres throughout the entire device. In this experiment, we used a mixture of 15 μm red fluorescent microspheres (Molecular Probes, #F-8842), 6 μm blue fluorescent microspheres (Polysciences, Inc. #19102-2), and 4 μm yellow-green fluorescent microspheres (Molecular Probes, #F-8859) to evaluate the sort-and-trap functionality of our device. The concentrations of the samples were 2.5 × 10^4 ml^{-1}, 10^4 ml^{-1}, and 10^4 ml^{-1} for 15 μm, 6 μm, and 4 μm microspheres, respectively. Whole device images in which different-sized particles were trapped in different zones, are shown in Fig. 5(a). To obtain a complete image of the device, several images from

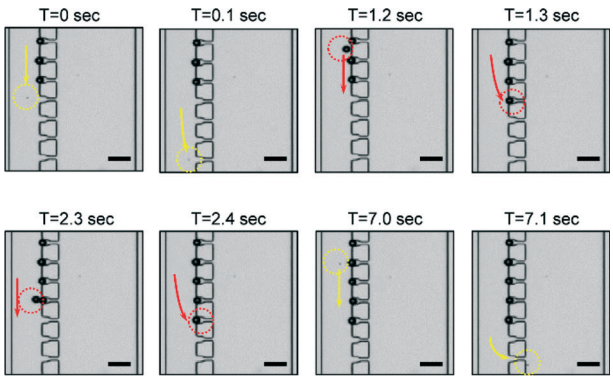

Fig. 4 Sequence of microsphere trapping by size. Scale bar: 50 μm.

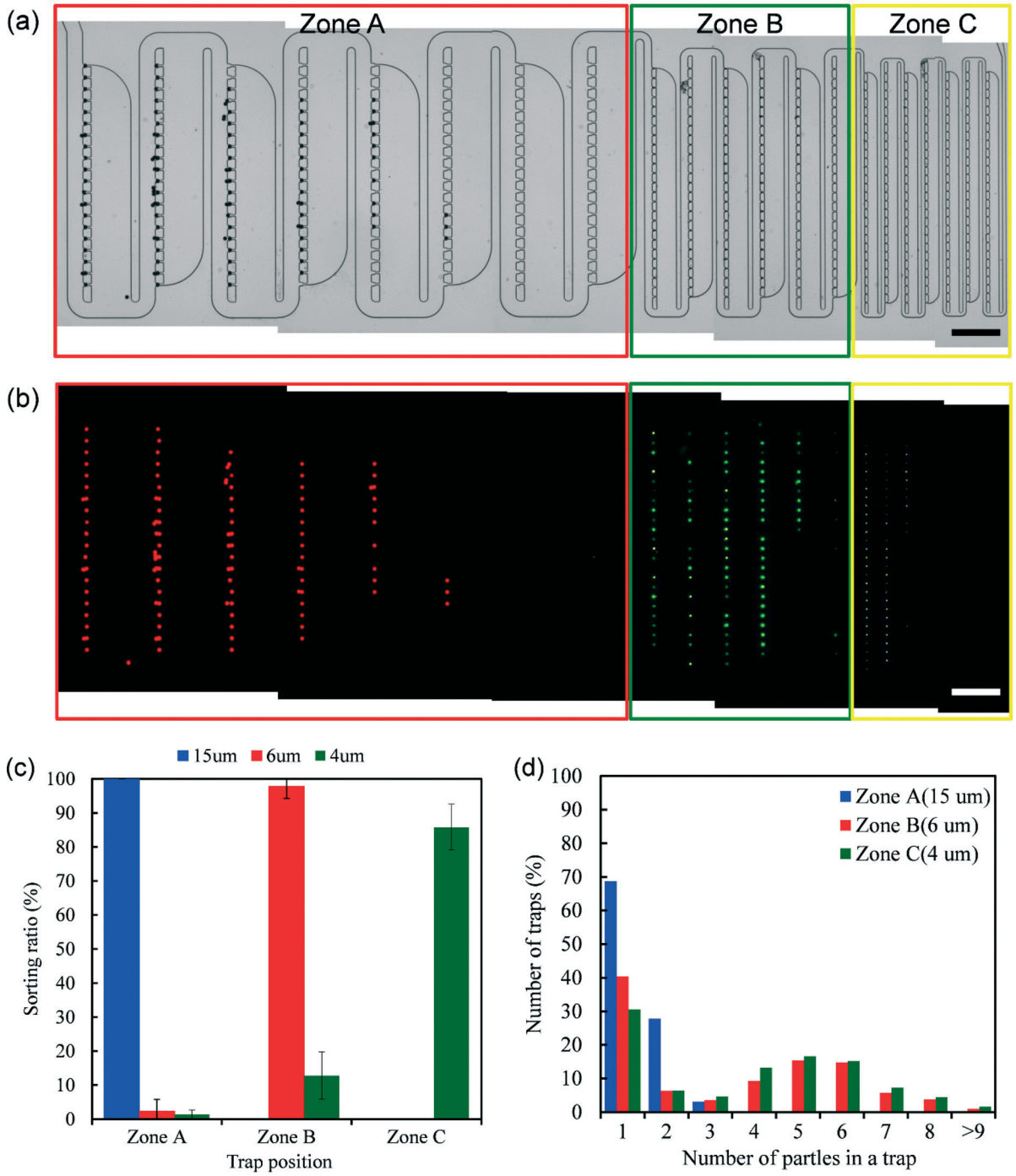

Fig. 5 Microsphere sorting and trapping experiment results. (a) Mixture of 15 μm, 6 μm, and 4 μm fluorescent microspheres sample. Red, yellow, and green rectangles represent zone A, B, and C, respectively. Scale bar: 200 μm. (b) Multi-channel fluorescence image of (a). Red, green, and yellow fluorescence signals originated from the 15 μm, 6 μm, and 4 μm microspheres, respectively. (c) Sorting efficiency by different size of microspheres counted from the fluorescence images (b). The error bar indicates the standard deviation of the sorting ratio from each experiment. (d) Distribution of the number of target microspheres in an occupied trap at each zone.

the camera were combined due to the limit of field of view from the objective lens (the individual images used for making complete device images are provided in the ESI†). From the multichannel fluorescence image [Fig. 5(b)], it is clear that different sized microspheres were successfully sorted by size and trapped at in the different zones. The use of differently labelled fluorescent microspheres in this experiment additionally allowed us to determine the number of particles captured at each trap based on the intensity of fluorescence. A trap with N fluorescent particles can be expected to be N times brighter than a trap with a single particle. We repeated the same experiment and gathered statistical data

to assess how much cross-trapping occurred between different zones. Fifty microliters of the mixture were inserted into the microfluidic channel at an infusion rate of 5 μl min^{-1}. We performed 10 repeated experiments and counted the particles trapped at each zone based on the fluorescence intensity. No loss of particles without trapping, was found during the experiments.

The trapping efficiency, defined as the ratio of the number of trapped particles to the sum of trapped particles and particles in the effluent is, to the best of our observation, 100%. This high trapping efficiency is consistent with our video observation (ESI† video), where we can see that the filling of the traps occur in an orderly sequential fashion and the particles rarely skip an unfilled trap during the filling process. For a particle to miss all the traps is a highly unlikely event.

To access how successfully different sized-microspheres are sorted by size in the device, we calculated sorting ratio for each microsphere defined as:

$$\text{Sorting ratio} = \frac{\#\text{ of same-type particles trapped in a region}}{\text{Total }\#\text{ of same-type particles trapped in the device}}$$

Result is shown in Fig. 5(c). During the experiments, every 15 μm microsphere trapped in the device was found in zone A. And almost 98% of 6 μm microspheres and 85% of 4 μm microspheres trapped in the device were seen in zone B and C, respectively. That means our device has at least 85% of sorting efficiency for the mixture of 15 μm, 6 μm and 4 μm microspheres. Most of the remaining 15% of the 4 μm microspheres were typically trapped in zone B, especially in the tiny gap near the already trapped 6 μm microspheres. This is mainly due to the multi-particle trapping in the small particle trapping zones, because small spheres can't fill the area perfectly. We checked the number of particles in an occupied trap for each zones. The result is shown in Fig. 5(d). Almost 70% of the traps in zone A were singly occupied with 15 μm microspheres while 40% of the traps in zone B and 30% of the traps in zone C were singly occupied with 6 μm and 4 μm microspheres, respectively. About 50% of traps in zone B and C were occupied by 4–7 particles. As a result, we need to consider this multi-trapping in the small particle trapping zone when deciding the number of necessary traps for each zone.

One of the applications of our sort-and-trap device is the detection and identification of waterborne parasites from infected water. We tested a mixture of 3 different types of waterborne parasite cysts (*Entamoeba histolytica*, *Giardia lamblia*, and *Cryptosporidium parvum*) for sorting and trapping with our device. The *Entamoeba* cyst has a spherical shape and 12–15 μm diameter, so we can expect it to be trapped predominantly in zone A. The *Giardia* cyst is an ellipsoid of 8 μm short axis and 19 μm long axis. We expect that it would flow within water with its long axis aligned with the flow direction in order to have minimum resistance. It should slip through the traps in zone A and be trapped in zone B. The *Cryptosporidium* cyst has a spherical shape and 3–5 μm diameter. As such we expect it to be trapped in zone C. Each parasite cyst was labelled with different fluorescence dyes for multichannel fluorescence imaging using monoclonal antibodies (*Entamoeba*: Alexa Fluor 488, *Giardia*: Alexa Fluor 350, and *Cryptosporidium*: Alexa Fluor 594). We prepared the mixture of *Entamoeba*, *Giardia*, and *Cryptosporidium* with concentrations of 2×10^4 ml^{-1}, 3×10^4 ml^{-1}, and 3×10^4 ml^{-1}, respectively. The sorting and trapping results using this biological sample mixture are shown in Fig. 6 (experimental condition was the same as before). From the multichannel fluorescence image of Fig. 6(b), we can check different parasite cysts were sorted by size and trapped at different zones. However, the fluorescence signals were too weak to get full device field of view, especially for the *Giardia* cysts. To obtain a stronger fluorescence signal, we used 10×/0.30 objective lens and collected fluorescence images from each part of traps in the device. The magnified bright field and fluorescence images at the positions indicated in Fig. 6(a) are shown in Fig. 6(c). The individual shapes of trapped cysts are able to be identified using the magnified bright field microscope images and the types of cysts are clearly distinguishable by magnified fluorescence images. The sorting ratios calculated from the 5 repeated experiments are shown in Fig. 6(d). Our device was able to sort the parasite cysts with good efficiency (almost 85% of sorting efficiency for three types of parasite samples). Furthermore, no single parasite cysts was observed in the effluent – the trapping efficiencies were uniformly high.

Discussion

In this paper, we implemented a microfluidic size sorting and trapping device for three different-sized particles. However, the levels of size sorting can exceed three, and continuously varying trap sizes can be made using similar methods. One item that we would like to address in future research is to achieve predominantly single trap occupancy throughout the whole system. This is desirable as it would simplify subsequent trapped particle counting. We note that the primary aim of this project is to design a microfluidic flow system that is capable of efficient sorting. We envision that achieving predominant single trap occupancy can be accomplishing in future works by tapering the channel height to match with the zone's target trapping size. Alternately, an accurate count can still be made with this prototype by collecting occupancy statistics *a priori*.

Our device employs sequential sorting method. As a result, its trapping capacity for each zone is determined by the number of traps. This means that once all the traps in the first zone are filled, the larger particles would start to fill the subsequent traps. This will skew any sorting analysis we try to do with the device. As such, the use of this type of devices for particle trapping and analysis would require putting in place an appropriate protocol to address this type of overfilling scenarios. One such protocol would be to reject the result of any assay in which the last 10% of any trap zones are filled. For samples that fail this criterion, we would require the user to

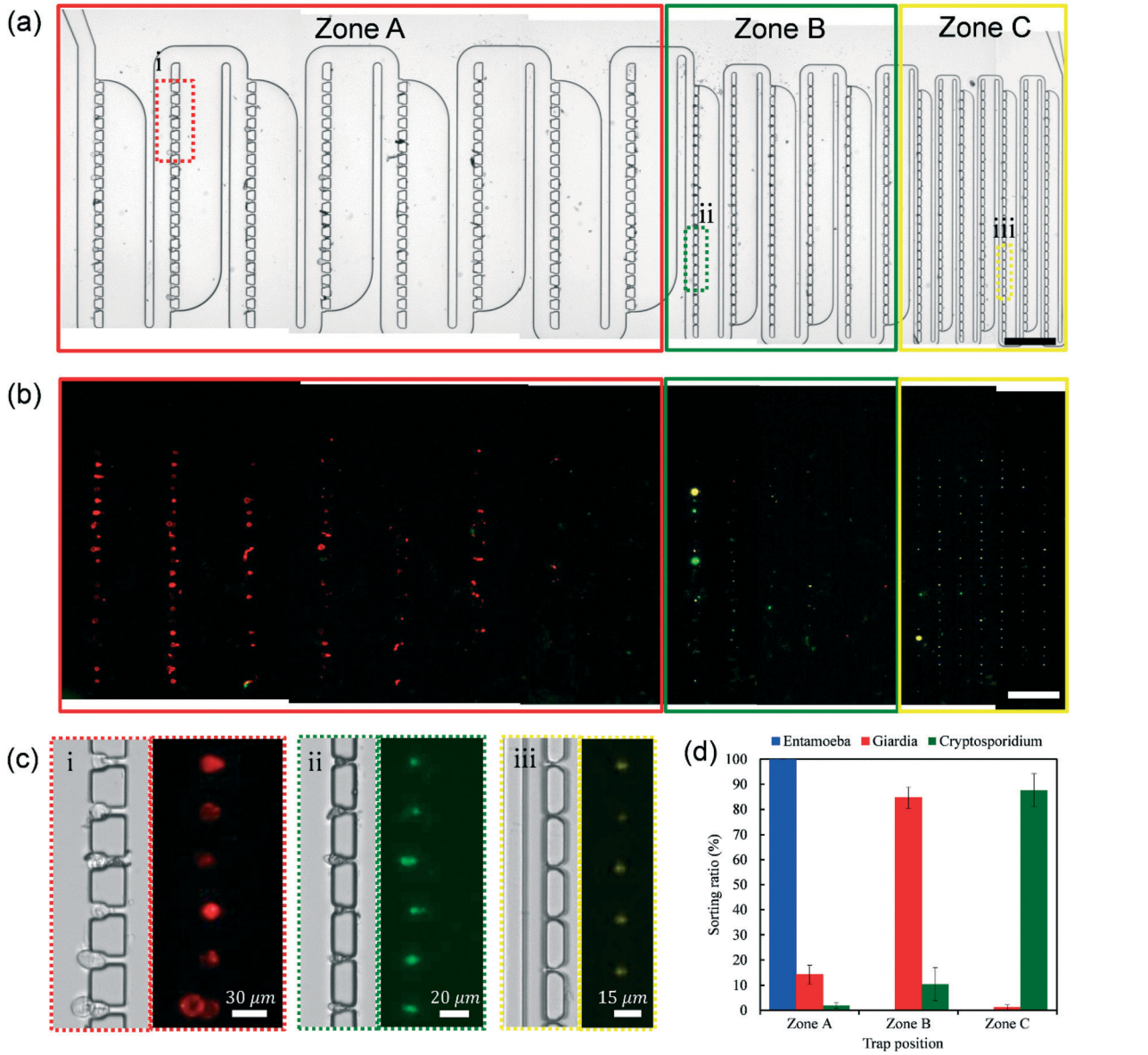

Fig. 6 Waterborne parasites sorting and trapping experiment results. (a) Mixture of *Entamoeba* (Alexa 488), *Giardia* (Alexa 350), and *Cryptosporidium* (Alexa 594). Scale bar: 200 μm. (b) Multi-channel fluorescence image of (a). (c) Magnified bright field and fluorescence images at the position indicated in (a). (d) Sorting efficiency by different parasites counted from the fluorescence images (c). The error bar indicates the standard deviation of the sorting ratio from each experiment.

use a device with more traps or operate multiple of the devices in multiplex.

There was a discrepancy between the number of particles in our sample solutions, and the actual particles trapped by the device and effluent. This is because at the low particle count and low sample volume with which we tested our device, a sizable fraction of the particles simply did not enter the device in the first place. This is why we believe the sum of particles in the effluent and the trapped particles is a much more reliable count of the particles that have actually entered the device. We expect a transport loss in tubing, sedimentation in a syringe, and inertial deposition in an inlet would be possible sources for particle loss during our sample loading.[18] While the inefficiency of actual particle input into the device does not impact the findings of this paper, we believe a key subsequent development would be to develop an appropriate technique or protocol to address this issue. One can either work on improving the proportion of particles flowing into the device, or alternately, perform appropriate data renormalization to account for the particle loss.

Finally, while our demonstration device does not allow for particle recovery after sorting, the simplicity of our microfluidic design is highly amenable to modifications to make sure recovery possible. For example, microfluidic valves can be used to isolate each zone and the contents can then be flushed out independently for examination.

Conclusions

We developed a microfluidic trap device that efficiently sorted and trapped particles by size. Fluid flow inside the microfluidic channel was calculated using CFD simulations, and optimum fluid flow for high particle trap efficiency was achieved by manipulating the sizes of channel widths. Due to fluid flow into the side channels, particles larger than the geometrical trap size were stuck inside the trap position, and particles smaller than the trap gap size passed through the trap position and moved into the next zone, until encountering a trap for their size. This sieve-like sorting was made possible by the periodic fluid flow patterns maintained inside the device regardless of trap size. For that purpose, we incorporated side channels inside the microfluidic device to prevent flow in one stage from disturbing fluidic flow patterns of the other stages. These side channels successfully decoupled the fluidic flows from different stages and made every flow pattern simple and controllable, regardless of the number and sizes of traps in each stage. Differently sized polystyrene microsphere samples and parasite cysts were used to assess the functionality of the device. Samples were successfully sorted into different zones by size and positioned at the traps in these zones.

Methods

Device fabrication

The microfluidic trapping device was made following the traditional microfluidic fabrication method.[17] First, SU-8 2015 (MicroChem) was spin-coated on a silicon wafer (2000 rpm, 30 s) and soft baked for 3 min at 95 °C. After exposure to UV light, the wafer was baked again for 5 min at 95 °C for a post-exposure bake (PEB). Development was made using the SU-8 developer for 3 min. The fabricated SU-8 mold was then placed inside a Petri dish. The PDMS (Sylgard 184) mixture at a ratio of 10 : 1 (base : curing agent) was poured onto the microfluidic channel mold. The Petri dish containing the PDMS and mold was kept inside a vacuum jar for 30 min to remove bubbles inside the PDMS mixture. After baking the PDMS in an oven for 30 min at 80 °C, the PDMS device was removed from the mold, and the inlet and outlet holes were punched. Fabricated PDMS microfluidic channels can be easily bonded to the slide glass after O_2 plasma treatment. The schematic for explaining the device fabrication can be found in the ESI.†

Sample preparation

Parasite cysts samples used in this paper were prepared following protocol. In a 96-well conical-bottom plate, incubate each parasite cyst in 200 μl blocking buffer (PBS with 10% (v/v) goat serum, 1% (w/v) bovine serum albumin, 100 mM glycine, and 0.05% (w/v) sodium azide) for 60 min at 37 °C. Then centrifuge at 3220*g* for 10 min at room temperature and remove supernatant. Resuspend cysts in 100 μl blocking buffer containing 1 : 100 mouse anti-cyst antibody (anti-*Giardia lamblia* cyst mouse monoclonal antibody IgG3 (Pierce, MA1-7741) and anti-*Cryptosporidium parvum* mouse monoclonal IgG1 antibody (MyBioSource, MBS320286)) and incubate for 60 min at 37 °C. Then centrifuge at 3220*g* for 10 min at room temperature and remove supernatant. Wash with 200 μl blocking buffer, centrifuge at 3220*g* for 10 min at room temperature and remove supernatant twice. Resuspend the cysts in 100 μl blocking buffer containing 1 : 100 $F(ab')_2$ fragment goat anti-mouse IgG (H + L) labelled with Alxea Fluor dyes (Invigrogen Molecular Probes, A11068, A10684, and A11020) and incubate for 60 min at 37 °C or overnight at 4 °C. Centrifuge at 3220*g* for 10 min at room temperature and remove supernatant. Then wash the cysts with 200 μl PBS and centrifuge at 3220*g* for 10 min at room temperature and remove supernatant twice. Before using the cysts for experiments, they are resuspended in PBS for specific concentration.

Acknowledgements

We would like to thank Seung Ah Lee for helpful advice on micro-fabrication. This project was funded by the National Institute of Health (NIH) Agency Award 1R01AI096226-01. Jinho Kim's work was supported by the Kwanjeong Educational Foundation.

Notes and references

1 A. R. Wheeler, W. R. Throndset, R. J. Whelan, A. M. Leach, R. N. Zare, Y. H. Liao, K. Farrell, I. D. Manger and A. Daridon, *Anal. Chem.*, 2003, **75**, 3581–3586.
2 R. M. Johann, *Anal. Bioanal. Chem.*, 2006, **385**, 408–412.
3 J. Nilsson, M. Evander, B. Hammarstrom and T. Laurell, *Anal. Chim. Acta*, 2009, **649**, 141–157.
4 D. Di Carlo, L. Y. Wu and L. P. Lee, *Lab Chip*, 2006, **6**, 1445–1449.
5 D. Wlodkowic, S. Faley, M. Zagnoni, J. P. Wikswo and J. M. Cooper, *Anal. Chem.*, 2009, **81**, 5517–5523.
6 W. H. Tan and S. Takeuchi, *Proc. Natl. Acad. Sci. U. S. A.*, 2007, **104**, 1146–1151.
7 W. H. Tan and S. Takeuchi, *Lab Chip*, 2008, **8**, 259–266.
8 S. Kapishnikov, V. Kantsler and V. Steinberg, *J. Stat. Mech.: Theory Exp.*, 2006, **2006**, P01012.
9 D. Huh, J. H. Bahng, Y. Ling, H.-H. Wei, O. D. Kripfgans, J. B. Fowlkes, J. B. Grotberg and S. Takayama, *Anal. Chem.*, 2007, **79**, 1369–1376.
10 M. Yamada, M. Nakashima and M. Seki, *Anal. Chem.*, 2004, **76**, 5465–5471.
11 J. Isaac-Renton, W. Moorehead and A. Ross, *Appl. Environ. Microbiol.*, 1996, **62**, 47–54.
12 M. L. Eberhard, N. J. Pieniazek and M. J. Arrowood, *Arch. Pathol. Lab. Med.*, 1997, **121**, 792–797.
13 F. M. White, *Fluid mechanics*, McGraw-Hill, New York, 1979.
14 K. Chung, Y. Kim, J. S. Kanodia, E. Gong, S. Y. Shvartsman and H. Lu, *Nat. Methods*, 2011, **8**, 171–176.

15 C. T. Crowe, *Multiphase Flow Handbook*, CRC Press, Boca Raton, 2006.
16 L.-S. Fan and C. Zhu, *Principles of Gas-Solid Flows*, Cambridge University Press, New York, 1998.
17 T. J. Levario, M. Zhan, B. Lim, S. Y. Shvartsman and H. Lu, *Nat. Protoc.*, 2013, **8**, 721–736.
18 S. L. von der Weiden, F. Drewnick and S. Borrmann, *Atmos. Meas. Tech.*, 2009, **2**, 479–494.

